Solar Energy 177 (2019) 155–162

Contents lists available at ScienceDirect

Solar Energy

journal homepage: www.elsevier.com/locate/solener

Techno-economic analysis of solar thermal power plants using liquid sodium as heat transfer fluid

Andreas Fritsch*, Cathy Frantz, Ralf Uhlig

German Aerospace Center (DLR), Institute for Solar Research, Pfaffenwaldring 38-40, 70569 Stuttgart, Germany

ARTICLE INFO

Keywords:
Concentrated solar power
Central receiver system
LCOE calculation
Molten salt
Liquid metals
Sodium

2010 MSC:
00-01
99-00

ABSTRACT

Solar thermal power plants with central receiver and thermal storage are expected to be one key technology in future electricity generation, because they are renewable and due to the thermal storage independent of the current solar radiation. State-of-the-art solar power plants often use molten nitrate salts as heat transfer fluid. The use of liquid sodium instead leads to lower electricity generation costs. Sodium has a high thermal conductivity and thus large heat transfer rates are possible. Hence, a smaller absorber surface is sufficient for the same thermal power. As a result, the sodium receiver achieves a higher efficiency at lower investment cost. Additionally, the aiming strategy, which reduces the peak heat flux on molten salt receivers isn't necessary for sodium. Even at high heat flux densities, the absorber tubes will be cooled sufficiently due to the high heat transfer coefficients. Therefore, the sodium receiver in this analysis is designed for one single aim point, resulting in a heat flux density of $\dot{q}_{mean}$ = 1.06 MW/m^2 and $\dot{q}_{peak}$ = 2.99 MW/m^2. The state-of-the-art system with molten salt considers $\dot{q}_{mean}$ = 0.51 MW/m^2 and $\dot{q}_{peak}$ = 1.0 MW/m^2. The presented techno-economic analysis of two sodium based concepts compared to a reference system with molten salt results in up to 16% lower electricity generation costs.

1. Introduction

Concentrating solar power (CSP) is a renewable energy option that uses concentrate sunlight to produce high temperature heat, which ca be used in a power block to generate electricity. The basic concept is illustrated in Fig. 1. Computer controlled mirrors (heliostats) follow the movement of the sun and reflect the sunlight to the receiver. Usually, the heliostat field surround the tower. In the receiver, the concentrated solar radiation is converted to heat and transferred to a heat transfer fluid (HTF). The energy in the fluid can be stored in tanks and transferred to water/steam by a steam generator to generate electricity in the turbine generator. Because CSP uses thermal energy, it can also incorporate thermal energy storage (TES) for higher levels of stability, dispatchability and increased duration of energy output. In June 2011, the Gemasolar plant already achieved 24 h uninterrupted electricity production (Burgaleta et al., 2011). Due to the low cost of molten salts this technology is on the advance. More than 70% of the plants under construction will use solar salt as HTF. However, the use of solar salt entails some disadvantages like the limited temperature range, corrosion and the operating behavior.

The Sunshot Initiative (Sunshot, 2014) of 2014 aims to reduce the levelized cost of electricity (LCOE) of such power plants to 0.06 $/kWh. In order to meet this goal further cost reduction is necessary. Basically, there are two options to reduce the LCOE:

- Higher overall efficiency (higher annual yield)
- Lower investment cost (direct cost reduction)

The use of liquid sodium as HTF in the solar receiver acts on both options to reduce the LCOE.

2. Advantages of sodium

The first advantage of sodium as HTF in solar power plants is its high temperature range in the liquid state (see Table 1). The low melting point of 98 °C leads to less trace heating compared to solar salt and therefore lower parasitic losses. On the other hand, sodium is suitable for high temperature high efficient energy conversion systems due to its high boiling point above 800 °C. Sodium is chemically stable and can even be operated at higher temperatures in the vapor state (e.g. Dish-Stirling engines Laing and Palsson, 2002 or AMTEC-cells de los Ríos Ramos et al., 2015). Binary salt mixtures like Solar Salt aren't chemically stable at higher temperatures. They can withstand temperatures around 600 °C, but the salt has to be replaced from time to

* Corresponding author.
E-mail address: Andreas.Fritsch@dlr.de (A. Fritsch).

https://doi.org/10.1016/j.solener.2018.10.005
Received 4 July 2017; Received in revised form 28 September 2018; Accepted 2 October 2018
Available online 14 November 2018
0038-092X/

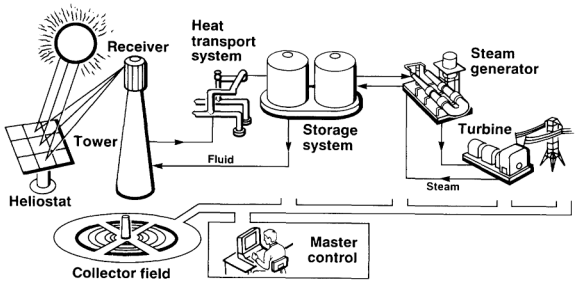

Fig. 1. Illustration of a solar thermal power plant with central receiver (Falcone et al., 1986).

Table 1
Cost data (Pacio et al., 2013) and temperature dependent physical properties of Solar Salt (60% $NaNO_3$ + 40% KNO_3) (Pacheco, 1995) and sodium (Fink and Leibowitz, 1995).

Heat transfer fluid (HTF)	Solar Salt	Sodium	Unit
Melting point	221	98	[°C]
Boiling point	~600	882	[°C]
Density ρ (290 °C)	1899	883	[kg/m^3]
Density ρ (565 °C)	1740	819	[kg/m^3]
Heat capacity c_p (290 °C)	1495	1313	[J/kg/K]
Heat capacity c_p (565 °C)	1538	1256	[J/kg/K]
Th. conductivity λ (290 °C)	0.50	76.0	[W/m/K]
Th. conductivity λ (565 °C)	0.55	61.1	[W/m/K]
Dyn. viscosity η (290 °C)	3.25	0.35	[mPa s]
Dyn. viscosity η (565 °C)	1.16	0.22	[mPa s]
Pr-number (290 °C)	9.73	0.006	[–]
Pr-number (565 °C)	3.26	0.004	[–]
Cost assumption	1.0	2.6	[€/kg]
Cost assumption	2.2	2.5	[€/dm^3]

time due to the decomposition process (Bauer et al., 2013). Another point is the compatibility with structural material. From literature corrosion problems are well known for salt mixtures, especially for high temperatures (Sequeira, 2003) whereas sodium shows no corrosion problems below the boiling point.

Another aspect is the heat transfer to the fluid. The thermal conductivity of sodium is over 100 times larger than with Solar Salt, resulting in very high heat transfer coefficients. This allows for flexibility in the design process of sodium receivers and very high heat flux densities can be achieved. For Solar Salt, the mean heat flux density is limited to ~ 0.5 MW/m^2 (see Vant-Hull Vant-Hull, 2002) and therefore the aperture area of the receiver is fixed. Due to the very high heat transfer coefficients with sodium, the receiver design can be adapted for low pressure drops whereas for Solar Salt high pressure drops are unavoidable for sufficient cooling of the absorber tubes.

The only disadvantage of sodium is its reactivity with water and oxygen which could result in fires that are difficult to extinguish. For this reason safety guidelines were developed already in the 1960s to avoid such accidents and to minimize damage in case of a sodium fire (Anderson, 1967). Unfortunately, not every sodium loop follows these guidelines and several sodium fires are reported in literature (e.g. the sodium fire on the Plataforma Solar de Almería (DFVLR, 1987) in 1986, which causes 30 years of abstinence of sodium in the solar community). Nevertheless, since 1950 a lot of experience was gained in the handling with sodium, especially in the nuclear power sector. The most important part of these construction guideline is the fail-drain-principle, which consists in early fail detection and then to drain fast all the liquid sodium into the sump tank. Additionally, driptrays have to be installed at the bottom of all components and all concrete surfaces have to be covered with sheet metal. The cold tramp and the cover gas argon are part of the safety system, too.

Currently, the biggest grid connected fast breeder reactor is the BN-800 in WNN (2015) with a power of 864 MW_{el}. During the last 30 years additional measurement technology was developed to early detect failures and further reduce risks. Recently, VastSolar built a grid connected solar thermal power plant with sodium as HTF (VastSolar, 2015).

3. Evaluated concepts

This article shows a techno-economic analysis of two plant configurations with sodium as HTF (Receiver only concept and tower loop) compared to a state-of-the-art molten salt system (reference). In all cases, external receivers with 360 °-Field are used. The comparison is made for large scale power plants (P_{el} = 125 MW) at the location Postmasburg, South Africa.

3.1. Reference system with Solar Salt

The large heat capacity and the low cost of molten salts make them attractive for direct storage. For this reason 'Solar Salt' was the choice of HTF in the Solar Two plant (1995) Pacheco (2002), in Burgaleta et al. (2011), NREL et al. (2017) and is the choice for most of the announced big solar thermal projects (NREL et al., 2017) (for example: Atacama-1, Chile with P_{el} = 110 MW; Redstone, South Africa with P_{el} = 100 MW; Copiapo, Chile with P_{el} = 260 MW; Supcon, China with P_{el} = 50 MW).

Therefore, the reference system in this article is based on a molten salt system (see Fig. 2). All sodium concepts are designed and calculated with the same tools and approaches and compared to this reference system.

3.1.1. Heliostat field

The heliostat field layout was optimized with the HFLCAL software (Schwarzbözl et al., 2009). An additional ray tracing software (SPRAY) was used to calculate the optical efficiency. The reflective area of one heliostat is 120 m^2 with a slope and tracking error of and $\sigma_{tracking}$ = 0.65 mrad. In order to reduce the peak heat flux and to get a more homogeneous heat flux distribution on the absorber multiple aim points are applied. This aim point strategy varies with the sun position minimizing the intercept losses. Table 2 shows the field efficiencies and the peak heat flux with and without aiming. The resulting field layout is presented in Section 5.

3.1.2. Receiver system

In the receiver, the solar radiation is transferred to heat. The receiver itself consists of several panels, which are arranged to a polygon thereby approximating a cylinder. Each of the panels consist of parallel tubes, through which the HTF is pumped during operation. These absorber tubes have to withstand high thermal gradients and stresses. Its design and arrangement is therefore crucial for the life span and the economic. The receiver of this calculation was designed with the ASTRID code (Frantz et al., 2016), which uses the heat flux distribution from the previously conducted ray tracing. The tubes considered for this calculation are simple stainless steel tubes (Inconel) without any additional structures or microchannels to enhance the heat transfer. This would result in lower peak temperatures and higher pressure drops, but also higher cost than simple tubes. The effect[1] of such design optimizations on the LCOE is much lower than that of the thermophysical properties of the HTFs (see Table 1). Within the ASTRID-code, heat transfer occurs due to the conduction within the tube wall and

[1] The effect of additional structures or microchannels are lower peak temperatures which allows higher heat flux densities and therefore higher receiver efficiencies, but on the other hand the higher pressure drop decreases the system efficiency and the higher manufacturing cost decreases the LCOE.

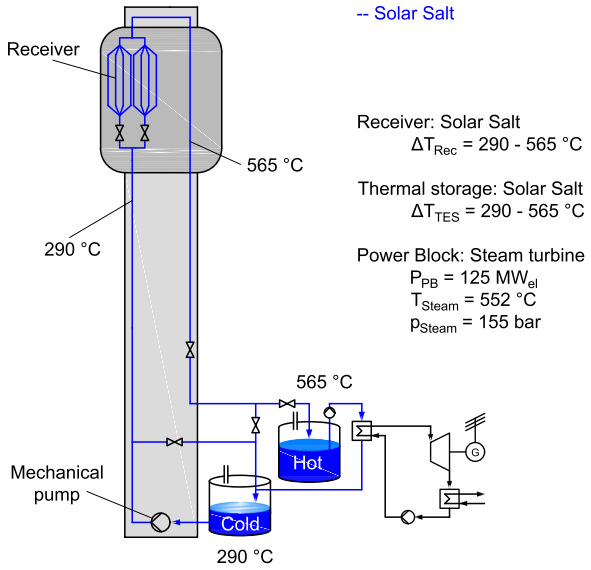

Fig. 2. Reference concept with Solar Salt as HTF and storage material. Power block with steam turbine and dry cooling.

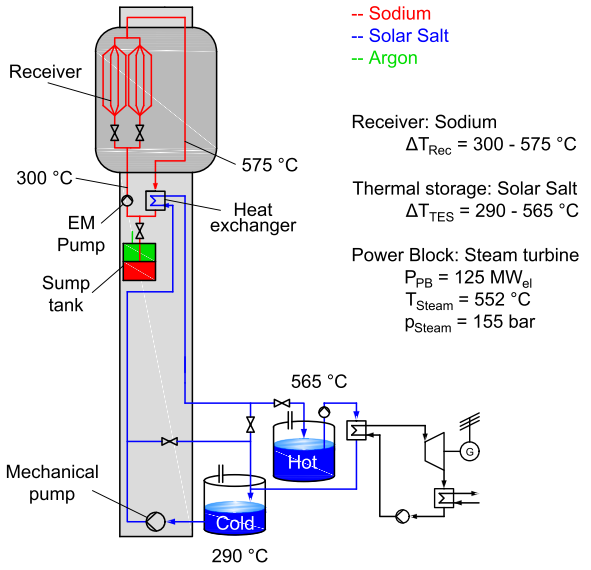

Fig. 3. Receiver-only concept with sodium as HTF in the receiver and heat exchanger to Salt as storage material. Power block with steam turbine and dry cooling.

Table 2
Optical efficiency and heat flux density on receiver surface (Reference system with Solar Salt, 700 MW_{th} receiver on 21 March)

Time	Azimut in [°]	Elevation in [°]	η_{field} (without aiming)	η_{field} (with aiming)
6h30	86.43	6.60	0.2755	0.2756
7h00	82.76	13.17	0.4331	0.4267
8h00	74.70	26.12	0.5818	0.5640
9h00	64.64	38.51	0.6292	0.6067
12h00	0	61.71	0.6760	0.6474
Peak heat flux density at 12h00:			2.23 MW/m^2	0.93 MW/m^2

conduction and convection within the HTF. The heat transfer coefficients are calculated with Nusselt number correlations. Radiation exchange between surfaces as well as natural and forced convection due to wind is also considered in the model. During the optimization process with FEM, the aperture size as well as the panel and tube number was varied. The resulting receiver geometry of this thermo-hydraulic optimization is presented in Section 5. During the design process, a maximum film temperature of 565 °C was considered for the Solar Salt receiver. For the sodium system, no temperature limit was set. The resulting tube temperatures are shown in Table 5. The panel arrangement is the same as in the Solar Two receiver with two flow paths and a cross section at half way through the receiver (Reilly and Kolb, 2001). The thermal energy storage operates at atmospheric pressure, thus the salt circulates in an open loop. The high tower height leads to a high head of the mechanical pumps, which represent a large proportion of the parasitic losses. This issue was considered within the field optimization.

3.1.3. Thermal energy storage (TES)

Despite the result, that one tank thermocline storage systems indicate lower cost (Pacheco et al., 2002), all commercial molten salt plants (see Section 3.1) are using 2-tank storage systems up to now. Therefore, all presented concepts consider a 2-tank storage system with Solar Salt. The storage size is optimized for each concept to minimize the LCOE.

3.1.4. Power block

Due to the temperature limitation of Solar Salt to 565 °C, a rankine cycle with steam turbine (125 MW_{el} with intermediate superheating to 552 °C at 155 bar) and dry cooling is used in this analysis. In the annual yield calculation, the turbine efficiency is calculated for each hour of the year depending on load and ambient temperature.

3.2. Receiver-only concept with sodium

The receiver-only concept is based on the reference system with Solar Salt. All components are identical except the receiver system, which is replaced by a sodium receiver and an additional heat exchanger to Solar Salt (see Fig. 3). In order to get the same temperature ranges in the thermal storage, the temperature of the sodium loop has to be increased by the temperature gradient between the two fluids. In the presented study, 10 K was supposed, resulting in a temperature range of 300–575 °C for the sodium loop.

As already discussed in Section 2, the use of sodium as HTF offers more flexibility in the receiver design. The aiming strategy isn't necessary anymore. Even at high heat flux densities, the absorber tubes will be cooled sufficiently due to the very high heat transfer coefficients of sodium. Therefore, one single aim point is applied in the middle of the sodium receiver. As a result, the aperture area of the absorber can be decreased without significantly reducing the field efficiency. Nevertheless, the tracking accuracy of the heliostats becomes more important with smaller receiver apertures.

Additionally, the sodium receiver can be designed for a lower pressure drop than the molten salt receiver. This low pressure drop allows the application of a EM pump which works without moving parts increasing the safety of the sodium loop. The efficiency characteristic of the EM pump used in the presented analysis was taken from (Ota et al., 2004).

3.3. Tower loop concept with sodium

A major part of the parasitic losses in the reference system and the receiver-only concept is due to the high head of the salt pump which works in an open loop, because the 2-tank storage is at atmospheric pressure. Typically, the salt is pumped up the tower and then throttled at the tower base before it enters the hot storage tank. The sodium receiver and the intermediate heat exchanger could be designed as a close loop system in which the work required to circulate the liquid metal is only due to the wall friction of the piping. In this case however, the intermediate heat exchanger has to be placed at the ground and riser and downcomer are filled with sodium. The 'tower loop' concept is

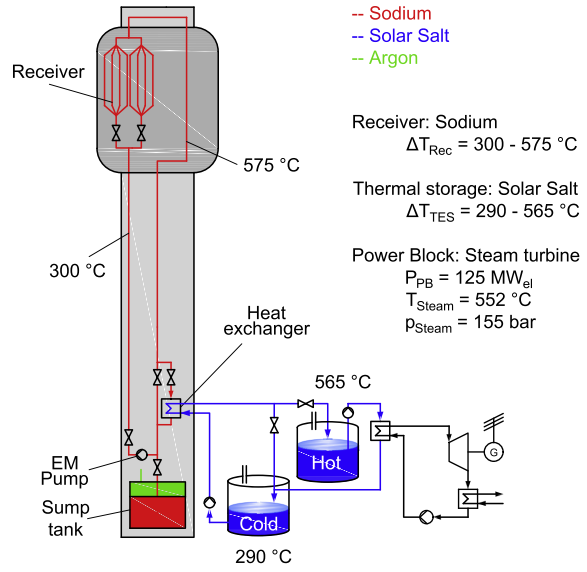

Fig. 4. Tower loop concept with sodium as HTF in the receiver. Riser and downcomer with sodium as well. Heat exchanger to Salt as storage material. Power block with steam turbine and dry cooling. Sump tank with capacity of all sodium in the loop. In case of leakage or maintenance all sodium will be drained to this sump tank.

designed in this way (see Fig. 4), resulting in further pumping reduction. As with the receiver-only and the reference concept, power block and thermal storage system stays unchanged.

4. Evaluation methodology

Fig. 5 shows the methodology for the concept assessment. As already mentioned, the field design is strongly dependent on the receiver design. The optimal receiver size depends on tracking accuracy, power, parasitics and cost. Reducing the absorber area results in higher receiver efficiency and lower receiver cost. But at the same time, this leads to higher spillage losses and therefore to a lower optical efficiency of the heliostat field, which increases the required number of heliostats and therefore the cost. In order to find the optimal trade-off between receiver size and optical efficiency a receiver aperture size study was conducted. For each receiver size, several iterations are necessary to get the optimal field layout and tower height.

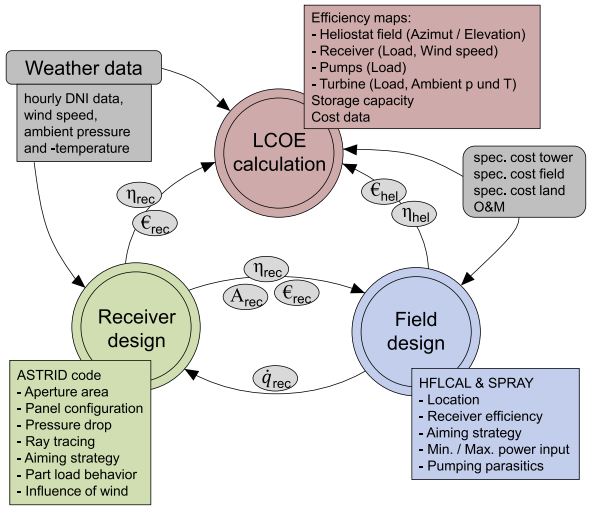

Fig. 5. Evaluation methodology and parameters used for the component design and annual yield and LCOE calculation.

4.1. Annual yield calculation

The annual energy yield is calculated by the sum of the hourly net electricity output of the power block during one year. The power block efficiency depends on the load and ambient temperature and pressure. The algorithm ignores the electricity demand from the grid and always tries full load operation (from storage or directly from receiver). The start-up energy for the receiver system and the power block is considered as well as parasitic losses (Pumps, trace heating, heliostat tracking). For each hour, the heat from the receiver is calculated by the DNI (time dependent), the reflective area of the heliostats (const.), the field efficiency (azimut, elevation) and the receiver efficiency (load, wind speed).

The capacity of the TES is optimized within the annual yield calculation to get the minimal LCOE (best ratio between storage size and energy dumping = defocus of heliostats).

4.2. Cost functions

The cost of the heliostat field ranges between 98 €/m^2 to 170 €/m^2 reflective area (Kolb et al., 2011). In the present analysis, the mean value of this range is used:

$$C_{\text{Field}} = 130€/\text{m}^2\text{mirror surface} + 3€/\text{m}^2\text{Land} \quad (1)$$

The tower height has a significant influence to the field efficiency but also to the parasitic losses due to pumping in the open salt loop. Commercial plants have tower heights between 100 and 200 m. This work uses the following tower height dependent cost function (Singer, 2014):

$$C_{\text{tower}} = 250,000 + 14.77 \cdot H_{\text{tower}}^{2.392} \quad [€] \quad (2)$$

The receiver system includes the panels with insulation, buffer and collection tank, the structural support as well as the equipment (pumps, valves, piping, compressor, trace heating, instrumentation and controls). Babcock (1984) estimates a cost break down for a four zone cavity. It turns out, that the biggest cost fraction is the erection with 44% of the total receiver cost. After transferring these cost data to a external molten salt receiver by introducing absorber area and power dependent cost functions as well as constant cost parameters, the following cost function for the receiver system was developed:

$$C_{\text{rec}} = \frac{46,438}{\bar{q}} + 21.899 \quad \left[€/\text{kW}\right] \quad (3)$$

The mean heat flux density $\bar{q}$ in [kW/m^2] is calculated by the quotient of thermal receiver power and the cylindrical surface of the receiver aperture. Fig. 6 shows this cost function.

The cost of the salt receiver of the reference system is therefore 115 €/kW, a value which is in the range of molten salt receiver cost data found in literature: Kolb et al. (2011): 96–154 €/kW, IRENA (IRENA, 2012): 116 €/kW.

The presented optimized sodium receiver results in a mean heat flux

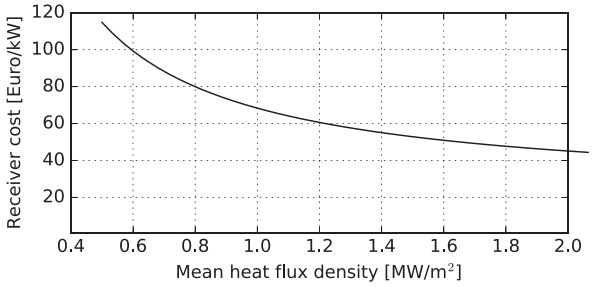

Fig. 6. Specific receiver cost function of external receivers with mean heat flux density $\bar{q}$ (quotient of thermal receiver power and the cylindrical surface of the receiver aperture).

of $\bar{\dot{q}} = 1.06\ \mathrm{MW/m^2}$ and therefore 66 €/kW receiver cost.

The liquid/liquid heat exchanger for sodium/Solar Salt is a safety-relevant component. In order to avoid the direct contact of sodium and Solar Salt, a double-tube safety heat exchanger is used in the analysis. The cost is estimated (Personal, 2015) to:

$$C_{HX} = 10.7140 \qquad [€/kW] \tag{4}$$

The cost of the 2-tank thermal storage system is developed in accordance to Fritsch et al. (2015) with E_{TES} as the storage capacity in MWh_{th}:

$$C_{TES} = 155.6 \cdot E_{TES}^{-0.3549} + 10.55 \qquad [€/kWh_{th}] \tag{5}$$

Based on the study by *Black* & *Veatch* for NREL (BV, 2012), the cost of the power block can be estimated to:

$$K_{PB} = 950 €/kW_{el} \tag{6}$$

Additional assumptions for financing, operation and maintenance used in the LCOE calculation are presented in Table 3.

5. Results

5.1. Heliostat field

Fig. 7 shows the field layout of the reference system with Solar Salt in comparison to the sodium system with the optical efficiency (color map) of each heliostat on 21.3 at 12 h. The field layout is strongly dependent on the receiver aperture size. The spillage increases with the distance between heliostat and receiver as well as with decreasing receiver sizes. The atmospheric attenuation also increases with the size of the heliostat field. From this point of view, the heliostats have to be placed as near as possible around the tower. However, blocking and shading of solar radiation increases, the narrower the heliostats are put together. The field optimization algorithm calculates the best compromise based on annual heat production cost. This means for the sodium system, that spillage dominates, resulting in a nearly circular field and heliostats are located very close to each other, accepting higher losses due to blocking and shading (see Fig. 7). Table 4 shows the optical efficiency of both heliostat fields.

5.2. Receiver comparison

The receiver can't be designed independently from the heliostat field, because there is a strong sensitivity between receiver, heliostat field and tower. Therefore, each plant has to be designed and optimized for the specific location and a detailed analysis with several iterations of field layout, ray tracing and receiver arrangement based on annual system performance is necessary. The receiver of the reference system with Solar Salt results in a mean heat flux density of $\bar{\dot{q}} = 0.51\ \mathrm{MW/m^2}$ with aiming strategy to limit the peak flux to approx. $\dot{q}_{peak} = 1.0\ \mathrm{MW/m^2}$. These values are in the range of all commercial molten salt power plants (e.g. Lata et al., 2008: $\bar{\dot{q}} = 0.48\ \mathrm{MW/m^2}$, SolarReserve, 2017: $\bar{\dot{q}} = 0.52\ \mathrm{MW/m^2}$). For liquid metal receivers no aim point strategy is necessary, resulting in a mean heat flux density of $\bar{\dot{q}} = 1.06\ \mathrm{MW/m^2}$ and a peak value of $\dot{q}_{peak} = 2.99\ \mathrm{MW/m^2}$. Table 5 shows the comparison of both receivers in detail. Although the receivers have the same thermal power, they differ significantly in size, weight and efficiency. The weight of the salt receiver absorber tubes is about 2.75 times higher than that of the sodium receiver. Despite the higher tube temperatures of the sodium receiver, the heat losses are lower because of the reduced absorber area. Additionally, the sodium receiver achieves very high Reynolds-numbers (≈ 10 times higher than for the salt receiver). In part load situations, the Reynolds-number decreases nearly linearly with the solar radiation. Therefore, the critical Reynolds-number (laminar flow) would be reached at lower radiation with the sodium receiver, increasing the operating time and the energy yield.

Another interesting aspect of the operating behavior is the retention time of the HTF in the receiver. The annual yield calculation of the presented analysis however ignores the dynamic behavior of the receiver. Instead, the calculation is based on the assumption that it's always possible to control the receiver outlet temperature to exactly 565 °C for Solar Salt and 575 °C for sodium. Additionally, a fixed start up energy is considered.

The receiver design indicates a significantly lower retention time in the sodium receiver of only 16 s towards 55 s for the Solar Salt receiver leads to advantages for the automatic control of the receiver. If gradients in the solar radiation occur (e.g. passage of clouds), the outlet temperature can be adjusted faster, especially in part load, where the inertia of the loop is still higher. Due to the imprecise forecast of cloud movement and the resulting heat flux distribution on the absorber tubes, receivers with Solar Salt operate in the so called *cloud standby* during cloudy sky to avoid overheating of the salt mixture. In this case, the mass flow is adjusted to achieve an outlet temperature of 510 °C under theoretical clear sky conditions (Zavoico, 2001). This safety mode reduces the energy yield. Sodium can be operated in the temperature range of 100–800 °C. For the operation between 290 and 565 °C neither freezing nor overheating precaution have to be implemented which increases the energy yield. The detailed analysis of dynamic receiver behavior and it's influence on the LCOE will be part of future work.

5.3. LCOE comparison

In all presented power plant concepts the same power block and storage system are applied. Due to this fact, the error of a relative LCOE comparison is minimized, because the cost assumptions of these components cancel each other out.

Table 6 summarizes the main plant parameters:

It turns out, that both sodium systems result in lower LCOE than the reference system with Solar Salt. The receiver-only concept results in up to 13% lower LCOE, whereas with the tower loop concept an LCOE reduction of 16% is achievable. Fig. 8 shows the comparison between the analyzed systems in terms of efficiency and investment cost. Table 7 summarizes additionally the detailed parasitic losses of the reference system and the sodium tower loop concept.

The higher annual energy yield of the sodium system is based on two features. Firstly the higher receiver efficiency and secondly the lower parasitic losses in the system (pumping and heat tracing). In the relative comparison of both systems, the gross efficiency of the sodium tower loop concept is 4% higher. Considering the parasitic losses, the sodium system results in a 9% higher net efficiency. The total system efficiency of the sodium system is therefore about 1.7%-points higher than that of the reference system.

The lower cost of the sodium system is to a small share due to the lower cost of the heliostat field (which is in fact a result of the higher system efficiency). The decisive cost reduction however is attained by the cost-effective sodium receiver. In total, the sodium system results in 8% lower investment cost.

Table 3
Cost parameters for financing, operation and maintenance (DLR)

Labor costs per employee	48,000 €/year
Number of persons (excl. field maintenance)	25 Pers.
Number of persons for field maintenance	0.03 Pers./1000 m^2
Water cost	200,000 €/year
O&M of equipment	3% of investment
Insurance cost	0.7% of EPC
Life time of plant	25 years
Dept interest rate i_r	8%
Fixed charge rate *FCR*	0.0937
Surcharges (engineering, risk, management)	35% of investment
Electricity consumption tracking heliostats	55 W_{el} per heliostat
Electricity from grid for offline parasitics	0.074 €/kW_{th}

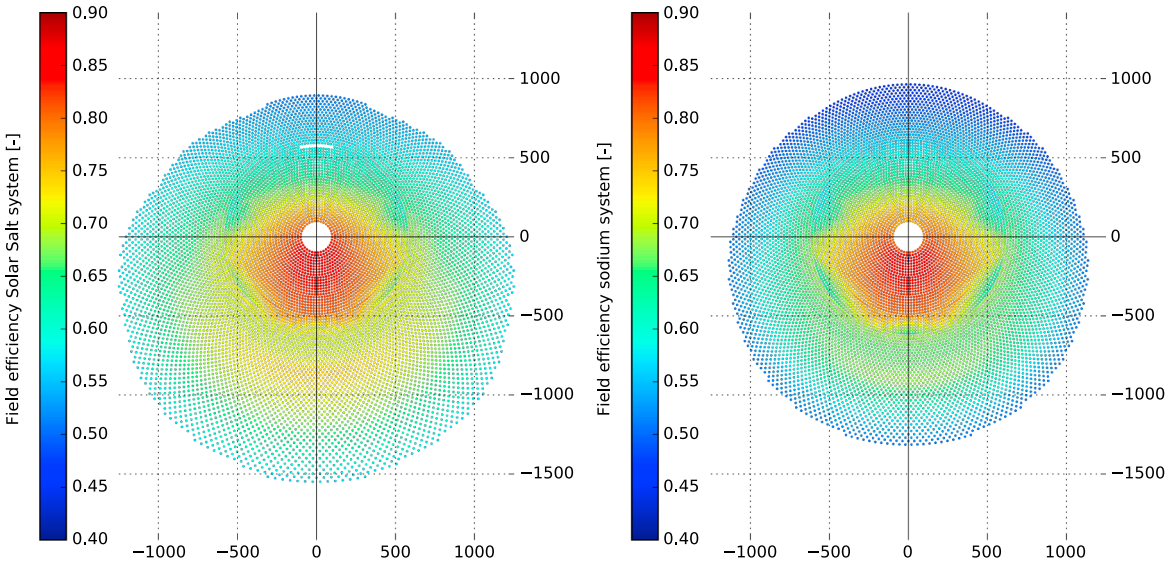

Fig. 7. Resulting field layout with optical efficiency on 21.3 at 12 h at Postmasburg in South Africa. The aperture size of one heliostat is 120 m^2. Left: Reference system with Solar Salt, thermal receiver power: 700 MW_{th}, Receiver size: 1376 m^2, number of heliostats: 10,137, tower height: 298 m. Right: Sodium system (receiver-only/tower loop), receiver power: 700 MW_{th}, Receiver size: 660 m^2, number of heliostats: 9897, tower height: 294 m.

Table 4
Results of field design (21.3. at 12 h): Comparison of field layout for two different receiver sizes with the same thermal power. Calculation made with ray tracing program SPRAY.

Configuration	Reference Solar Salt	Sodium system
Thermal power	700 MW_{th}	700 MW_{th}
Receiver size (aperture)	1376 m^2	660 m^2
Tower height	298 m	294 m
Number of heliostats	10,137	9897
Reflectivity of mirrors	89.3%	89.3%
Field efficiency	21.3./12 h	21.3./12 h
Cosine efficiency	86.6%	85.7%
Blocking & shading	96.8%	96.1%
Extinction	90.4%	90.1%
Intercept	95.6%	97.5%
Total field efficiency	64.8%	64.7%
Peak heat flux	0.93 MW/m^2	2.99 MW/m^2

Table 5
Receiver comparison between Reference system with Solar Salt and Sodium system (Receiver-only and Tower loop)

Configuration	Reference Solar Salt	Sodium system
Absorber surface (cylinder) [m^2]	1376	660
Number of panels [–]	2 × 5	2 × 3
Pressure drop in receiver[b] [bar]	13.16	1.87
Number of tubes[a] per panel [–]	142	131
Inner tube diameter [mm]	32.8	50
Tube wall thickness [mm]	1.4	1.4
Total weight of empty tubes [t]	65	24.1
Total weight of HTF in receiver [t]	82.3	29.4
Min./Max. flow velocity[b] [m/s]	3.8/4.2	4.4/4.6
Min. Reynolds number[b] [–]	68000	569 000
Min./Max. heat trans.coeff.[b] [$kW/m^2/K$]	7.9/12.7	29.2/32
Retention time of HTF in receiver[b] [s]	55	16
Receiver inlet temperature [°C]	290	300
Receiver outlet temperature [°C]	565	575
Max. tube wall temperature[c] [°C]	628	689
Max. heat flux density[b] [MW/m^2]	0.93	2.99
Absolute absorptivity[be] [%]	94.8	94.7
Absorbed heat by tubes[b] [MW_{th}]	721.4	711.7
Heat transferred to fluid[b] [MW_{th}]	699.7	699.9
Total heat losses[b] [MW_{th}]	42.5	27.4
Receiver efficiency[bd] [%]	91.9	93.1
Diameter riser/downcomer [m]	0.6	0.6
Max. static pressure in riser [bar]	59.1	26.4
Pressure drop in riser/downcomer[b] [bar]	0.56	1.09

[a] Tube material: INCONEL alloy 617.
[b] On 21 March at 12 h.
[c] On 21 March at 9 h.
[d] Absorbed by sodium/Incident on tubes.
[e] Absorptivity of tube material (coating): 0.93.

The tracking accuracy of the heliostat field is essential for the presented results. Changes in slope and tracking errors of the heliostats may result in other results. For this reason, a sensitivity analysis was conducted. The slope and tracking error was increased by 50%, representing a heliostat field with low accuracy and subsequently decreased by 25% for high precision heliostats.

The high precision heliostat field results obviously in smaller receiver apertures and lower LCOE. But even with low precision heliostats (σ_{slope} = 1.95 mrad and $\sigma_{tracking}$ = 0.975 mrad), the optimized receiver aperture size is still ≈ 25% lower than the reference case and the LCOE reduction with the sodium tower loop is about 12%.

6. Conclusions and outlook

The paper discusses two different sodium based solar tower concepts in comparison with a state-of-the-art molten salt system. The conducted techno-economic analysis turns out in significant lower electricity generation costs for both sodium systems. Up to 16% lower LCOE are achievable with the sodium tower loop concept. This result must be confirmed by the construction of real power plants.

The design of sodium receivers differ significantly from molten salt receivers. Further optimization is still possible. One research path is the panel arrangement and their conjunction. The presented sodium receiver design is similar to a molten salt receiver. Other arrangements with double-sided irradiated tubes and/or mass flow controlled panels with the total temperature difference (290–565 °C) within each panel are promising concepts for high flux and high efficient receivers. Another research path is the dynamic behavior of the receiver system, including the temperature control during fluctuating irradiation and the start up and shut down process as well. The volume change during

Table 6
Summary of plant configuration with main parameters

Configuration	Reference Solar Salt	Sodium Tower loop
Plant location	South Africa, Postmasburg	
Number of heliostats (each 121 m^2)	10,137	9897
Field size	6.1 km^2	5.2 km^2
Solar multiple	2.52	2.38
Tower height	316 m	306 m
Receiver aperture	1376 m^2	660 m^2
Receiver power	700 MWth	
Storage size	11.6 h	11.4 h
Storage size	3.415 GWh	3.356 GWh
Design gross el. output	125 MWel	
Design gross efficiency power block	42.46%	

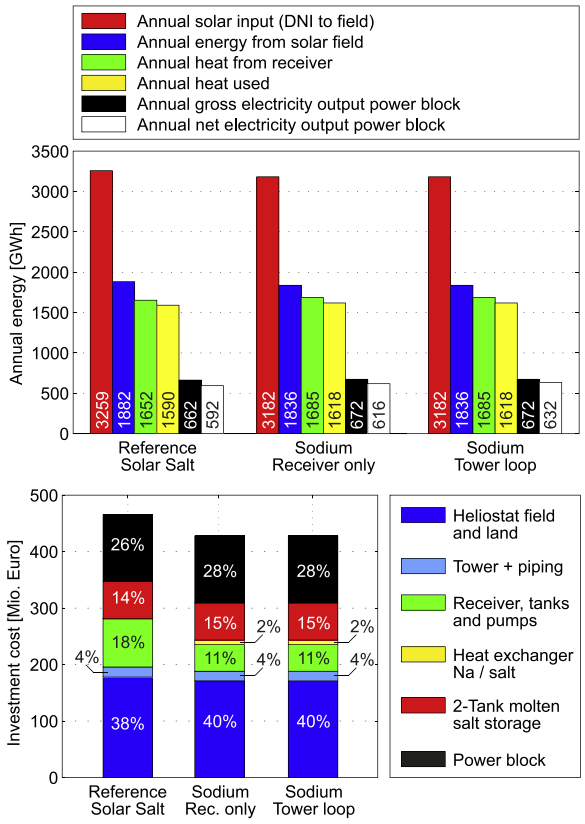

Fig. 8. Top: Annual energy conversion and efficiency for all concepts. Bottom: Investment cost breakdown (absolute and ratio).

phase change from solid to liquid is for sodium about four times lower than for Solar Salt (Boerema et al., 2015). The daily freezing of sodium during night with solar thawing in the morning could be possible without decreasing the absorber life time. This feature of sodium would additionally decrease the power consumption for trace heating and extend the energy collection.

Finally, other power block configurations with higher temperatures and higher efficiencies (Brayton cycle/CO_2-turbine) can further reduce the electricity generation costs of solar power plants.

Acknowledgments

The authors wish to acknowledge the support of the Helmholtz Association in the framework of the Helmholtz-Alliance LIMTECH (Liquid Metal Technology), Subtopic B2: Liquid Metals for Solar Power Systems.

Table 7
Comparison of annual efficiencies and total cost between reference system Solar Salt and Sodium tower loop. HX = heat exchanger, SG = steam generator.

Configuration	Reference Solar Salt	Sodium Tower loop
Efficiency heliostat field [%]	57.75	57.70
Receiver efficiency [%]	87.78	91.79
Energy losses (Storage, dumping, …) [%]	96.23	96.02
Turbine efficiency [%]	41.62	41.54
Parasitics (Pumps, trace heating) [%]	89.47	93.99
Pump receiver loop + HX [GWh]	21.97	2.32
Pump salt (HX + SG) [GWh]	0.90	1.59
Parasitics in power block [GWh]	28.43	29.27
Trace heating [GWh]	18.31	6.38
Total efficiency [%]	18.16	19.86
Cost heliostat field + tower [Mio.€]	177.7	171.2
Cost land [Mio.€]	17.9	16.9
Cost receiver system + HTF [Mio.€]	85.5	47.3
Cost heat exchanger [Mio.€]	0	8.0
Cost thermal storage [Mio.€]	65.6	65.6
Cost power block [Mio.€]	118.8	118.8
Indirect Cost [Mio.€]	162.9	149.7
Total cost [Mio.€]	465.5	427.7

References

Anderson, F.A., 1967. A primer for the safe use of liquid alkali metals. Oak Ridge National Laboratory, U.S. Atomic energy commission, oRNL-TM-1740.
Babcock, 1984. Wilcox, Molten Salt Receiver Subsystem Research Experiment – Executive Summary, Department of Energy, Sandia National Laboratories, Albuquerque, New Mexico 87185 and Livermore, California 94550, sAND84-8178.
Bauer, T., Pfleger, N., Breidenbach, N., Eck, M., Laing, D., 2013. Material aspects of solar salt for sensible heat storage. Appl. Energy 111, 1114–1119. https://doi.org/10.1016/j.apenergy.2013.04.072.
Boerema, N., Taylor, R.A., Morrison, G., Rosengarten, G., 2015. Solid-liquid phase change modelling of metallic sodium for application in solar thermal power plants. Sol. Energy 119, 151–158.
Burgaleta, J.I., Arias, S., Ramírez, D., 2011. Gemasolar, the first tower thermosolar commercial plant with molten salt storage. In: SolarPaces International Conference, Marrakech.
BV, 2012. Cost and performance data for power generation technologies, Black & Veatch, prepared for the National Renewable Energy Laboratory NREL (February 2012).
de los Ríos Ramos, N.D., Onea, A., Scherrer, S., Weisenburger, A., Hering, W., 2015. Direct energy conversion of heat to electricity using amtec, European Union 978-1-4673-7172-8/15.
Deutsche Forschungs- und Versuchsanstalt für Luft- und Raumfahrt DFVLR, Lessons from the SSPS-CRS sodium fire incident, motor Columbus (März 1987).
DLR, 2014. Internal data of the german aerospace center, Institut of solar research, Point focusing systems.
Falcone, P.K., 1986. A handbook for solar central receiver design. Department of Energy, Sandia National Laboratories Livermore, sAND86-8009.
Fink, J.K., Leibowitz, L., 1995. Thermodynamic and transport properties of sodium liquid and vapour. Argonne National Laboratory, Reactor Engineering Division, aNL/RE-95/2.
Frantz, C., Fritsch, A., Uhlig, R., 2016. Astrid - advanced solar tubular receiver design: a powerful tool for receiver design and optimization. In: Proceedings SolarPaces International Conference, Abu Dhabi.
Fritsch, A., Flesch, J., Geza, V., Singer, C., Uhlig, R., Hoffschmidt, B., 2015. Conceptual study of central receiver systems with liquid metals as efficient heat transfer fluids. Energy Procedia 69, 644–653.
IRENA, 2012. Renewable energy technologies: cost analysis series, Concentrating Solar Power, The International Renewable Energy Agency, volume 1: Power Sector, Issue 2/5.
Kolb, G.J., Ho, C.K., Mancini, T.R., Gary, J.A., 2011. Power Tower Technology Roadmap and Cost Reduction Plan. Department of Energy, Sandia National Laboratories, Albuquerque, New Mexico 87185 and Livermore, California 94550, sAND2011-2419.
Laing, D., Palsson, M., 2002. Hybrid dish/stirling systems: combustor and heat pipe receiver development. J. Sol. Energy Eng. Trans. ASME 124, 176–181.
Lata, J.M., Rodríguez, M., de Lara, M.A., 2008. High flux central receivers of molten salts for the new generation of commercial stand-alone solar power plants. Sol. Energy Eng. 130, 1–5.
NREL, 2017. Concentrating solar power projects database. National Renewable Energy Laboratory Web page, last visit: Jan. 25, 2017. <https://www.nrel.gov/csp/solarpaces/>.
Ota, H., Katsuki, K., Funato, M., Taguchi, J., Fanning, A.W., Doi, Y., Nibe, N., Ueta, M.,

Inagaki, T., 2004. Development of 160m^3/min large capacity sodium-immersed selfcooled electromagnetic pump. Nucl. Sci. Technol. 41, 511–523.
Pacheco, J.E., 1995. Results of Molten Salt Panel and Component Experiments for Solar Central Receivers, Department of Energy, Sandia National Laboratories, Albuquerque, New Mexico 87185 and Livermore, California 94550, sAND1994-2525.
Pacheco, J.E., 2002. Final Test and Evaluation Results from the Solar Two Project, Department of Energy, Sandia National Laboratories, Albuquerque, New Mexico 87185 and Livermore, California 94550, sAND2002-0120.
Pacheco, J.E., Showalter, S.K., Kolb, W.J., 2002. Development of a molten-salt thermocline thermal storage system for parabolic trough plants. J. Sol. Energy Eng. 124, 153–159.
Pacio, J., Singer, C., Wetzel, T., Uhlig, R., 2013. Thermodynamic evaluation of liquid metals as heat transfer fluids in concentrated solar power plants. Appl. Therm. Eng. 60 (1–2), 295–302. https://doi.org/10.1016/j.applthermaleng.2013.07.010.
Personal conversation with Deller GmbH and cost estimation of a double-tube safety heat exchanger for sodium/Solar Salt, Wilhelm Deller heat exchangers, Siegen, summer 2015.
Reilly, H.E., Kolb, G.J., 2001. An Evaluation of Molten-Salt Power Towers Including Results of the Solar Two Project, Department of Energy, Sandia National Laboratories, Albuquerque, New Mexico 87185 and Livermore, California 94550, sAND2001-3674.
Schwarzbözl, P., Pitz-Paal, R., Schmitz, M., 2009. Visual hflcal - a software tool for layout and optimisation of heliostat fields. In: Proceedings SolarPaces International Conference, Berlin.
Sequeira, C., 2003. Fundamentals of molten salt corrosion, Molten Salt Forum, Trans Tech Publication, Switzerland, vol. 7, pp. 3–40.
Singer, C., 2014. Assessment of improved molten salt solar tower plants, SolarPaces 2013. Energy Procedia 49, 1553–1562.
SolarReserve, 2017. Crescent dunes solar energy project, SolarReserve Web page, last visit: May 2017. <http://www.solarreserve.com/en/technology/molten-salt-tower-receiver>.
Sunshot, 2014. Tackling challenges in solar: 2014 portfolio. Tech. Rep. DOE/EE-1081, U. S. Department of Energy: Sunshot Initiative, Solar Energy Technologies Office.
Vant-Hull, L.L., 2002. The role of allowable flux density in the design and operation of molten-salt solar central receivers. J. Sol. Energy Eng. 124, 165–169. https://doi.org/10.1115/1.1464124.
VastSolar, 2015. Commercially sustainable csp scalable, high efficiency, low cost. In: ASTRI Symposium (11. Februar 2015).
WNN, 2015. Russia connects bn-800 fast reactor to grid, World Nuclear News Web page, last visit: 11. Dezember 2015. <http://www.world-nuclear-news.org/NN-Russia-connects-BN800-fast-reactor-to-grid-11121501.html>.
Zavoico, A.B., 2001. Solar Power Tower Design Basis Document, Department of Energy, Sandia National Laboratories, Albuquerque, New Mexico 87185 and Livermore, California 94550, sAND2001-2100.